Measuring signatures in photon angular spectra to distinguish nonlinear Compton scattering models

Brandon K. Russell,[1,*] Stepan S. Bulanov,[2] Qian Qian,[1] Christopher Arran,[3] Thomas G. Blackburn,[4] Sergei V. Bulanov,[5,6] Gabriele M. Grittani,[5] Stuart P. D. Mangles,[7] Christopher P. Ridgers,[3] Daniel Seipt,[8,9] and Alexander G. R. Thomas[1]

[1] *Gérard Mourou Center for Ultrafast Optical Science, University of Michigan, 2200 Bonisteel Boulevard, Ann Arbor, Michigan 48109, USA*
[2] *Lawrence Berkeley National Laboratory, Berkeley, California 94720, USA*
[3] *Department of Physics, York Plasma Institute, University of York, York YO10 5DD, United Kingdom*
[4] *Department of Physics, University of Gothenburg, SE-41296 Gothenburg, Sweden*
[5] *ELI Beamlines Facility, The Extreme Light Infrastructure ERIC, Za Radnicí 835, Dolní Břežany, 25241, Czech Republic*
[6] *National Institutes for Quantum and Radiological Science and Technology (QST), Kansai Photon Science Institute, Kyoto, 619-0215 Japan*
[7] *The John Adams Institute for Accelerator Science, Imperial College London, London, SW7 2AZ, UK*
[8] *Helmholtz Institute Jena, Fröbelstieg 3, 07743 Jena, Germany*
[9] *GSI Helmholtzzentrum für Schwerionenforschung GmbH, Planckstraße 1, 64291 Darmstadt, Germany*

(Dated: December 2, 2024)

The collision of a high energy electron beam with a laser pulse may be used to study radiation reaction and nonlinear Compton scattering among many other processes in strong field quantum electrodynamics. Predictions from simulation and theory for these interactions rely on a number of approximations and assumptions that have not been experimentally tested. Here, experimentally measurable signatures are identified that might be able to distinguish between radiation reaction models, i.e., classical or quantum, or between the local constant field and local monochromatic approximations used to calculate the properties of the nonlinear Compton process. These signatures are considered through Monte Carlo simulations of various experimental conditions that are relevant to today's laser facilities. Potential detection schemes for measuring the signatures are proposed. We find that single photon counting of keV photons to resolve harmonics and scintillator based detection of MeV photons may allow us to validate nonlinear Compton scattering models and radiation reaction models respectively. This will require electron beams with divergence angles less than 2 mrad and less than 20% energy spread.

I. INTRODUCTION

The emergence of multi-petawatt class laser systems [1] has sparked significant interest in a set of widely recognized theoretical challenges related to the interaction between strong electromagnetic fields and relativistic electron beams [2–5], which have yet to be fully validated through experimentation. In particular, two important low order quantum processes are the emission of a photon by a charged particle and the decay of a photon into an electron positron pair in a strong electromagnetic field. These processes are known by different names in different contexts, but in the interaction of leptons with extremely intense laser pulses these are known as, respectively, nonlinear Compton scattering (NLCS) and nonlinear Breit-Wheeler (NLBW) pair creation. These processes are of fundamental interest, being related to photon generation and pair production mechanisms that are expected to occur naturally in our universe, but only in the most energetic environments, such as within strongly magnetized regions surrounding magnetars [6] and in pulsar magnetospheres. Additionally, they are important for understanding the physics of matter in the foci of new multi-petawatt ultra-intense laser facilities [7–11] that will make the experimental study of strong-field quantum electrodynamic (SF-QED) effects possible [3, 4]. Validation of the models for these processes is important as they are a fundamental component of the simulations in extreme astrophysics [12, 13] and laser-plasma interactions with multi-petawatt lasers [14].

The linear versions of these processes are theoretically calculated and experimentally confirmed to high precision [15]. However, in the nonlinear regime the usual QED perturbation techniques break down and it is instead typical to use Volkov states [16] to recast the problem as a new perturbation theory using these "dressed" states [17–19], which has less experimental data in support. In strong fields, the two important nonlinearity parameters are the classical parameter $a_0 = e\sqrt{-A_\mu A^\mu}/m_e c$, which is the amplitude of the dimensionless vector potential of the electromagnetic field[20], and the quantum parameter $\chi = |F^{\mu\nu}p_\nu|/m_e E_s$. Here, $F^{\mu\nu} = \partial_\mu A_\nu - \partial_\nu A_\mu$ is the electromagnetic field tensor, A_μ is the electromagnetic field four-potential, p_ν is the particle four-momentum, e and m_e are electron charge

* bkruss@umich.edu

and mass respectively, and $E_s \approx 1.32 \times 10^{18}$ V/m is the critical field of QED or Schwinger field. Pioneering measurements were made at the SLAC E-144 experiment in the very weakly nonlinear regime where standard perturbation theory may still be applied [21, 22]. In the supporting theoretical calculations an adiabatic assumption was made that the local rate was that of the infinite plane wave with equivalent χ, which was later formalized as the "locally monochromatic approximation" (LMA) [23].

In the strongest laser fields corresponding to multi-petawatt laser facilities for which $a_0 \gg 1$, particles may be accelerated to very high energies by the field strength such that the fields in their rest frame are close to crossed E and B fields, and the coherence length for the formation of the photon is extremely short such that they can be treated as approximately constant; i.e., the "locally constant crossed-field approximation" (LCFA). Recently, NLCS experiments were performed using laser wakefield accelerated electron beams at higher laser field strength [24, 25] than the SLAC E-144 experiments. While these experiments showed evidence for quantum radiation reaction (a manifestation of NLCS), limited data and significant noise made this dataset insufficient to constrain the NLCS model to determine deviations from the LCFA.

In NLCS, a very large number of laser photons are absorbed by a single lepton and a single high-energy photon is emitted, i.e., $e^- + n\gamma \rightarrow e^- + \gamma'$ [19]. The probability of this process occurring depends on the parameter χ_e, with larger χ_e making the process more probable. Due to the fact that the parameter χ_e depends both on the field strength and the momentum of an electron, the head-on collision of this electron and the laser maximizes the value of χ_e. In this case $\chi_e \simeq 2\gamma E/E_S$, where γ is the electron Lorentz factor.

Head-on collision experiments have focused on finding signatures of radiation reaction (the change in momentum a particle experiences as it emits photons) in the electron and photon energy spectra. Classical electrodynamics addresses this problem by describing the electron propagation in the electromagnetic field by using the equation of motion with both the Lorentz force and the classical radiation reaction (CRR) force taken into account, where the CRR force is determined from the ensemble averaged amount of momentum radiated by an electron along its trajectory. In this case a nonphysical photon spectra where photon energies exceed the energy of the electrons is predicted. This leads to an overestimate of the electron energy loss among other effects. Quantum radiation reaction (QRR) is usually referred to as the recoil coming from the sequential, incoherent emission of many photons (see e.g. [2, 4, 5]), where the electron motion between these emission is governed by an equation of motion with just the Lorentz force taken into account. The differences between CRR and QRR manifest themselves in different electron and photon energy spectra. However, if a_0 is large such that there is significant photon production and χ_e is small such that these photons are low energy, then the difference will be negligible. The over-estimate in the radiated power by CRR compared to QRR is given by the inverse of the Gaunt factor [26, 27].

In addition to measuring differences between CRR and QRR, it is also important to validate the models used to calculate the probabilities of each of these photon emissions, i.e., NLCS, in the QRR case: the LCFA and the LMA. The LCFA is the main model used in the popular particle-in-cell (PIC) codes, allowing for NLCS to be simulated in plasmas. The LCFA and the LMA predict similar photon spectra at high energies. However, below keV energies the models diverge as the LCFA greatly over predicts the photon number as the underlying assumption of incoherent photon emission breaks down [28]. Measuring these differences in the energy spectra in the QED regime is non-trivial and so far has not been achieved. Note, that the LMA is better suited to interactions with $a_0 \lesssim 20$ because of the increasing complexity of the calculations, while the LCFA is accurate only for frequencies above $\omega_{inc} \sim \gamma^2\omega_0/a_0^2$, if $a_0 \gg 1$. This is because the LCFA requires incoherent emission where the photon formation length is smaller than the oscillation period of the electron in the laser field [29].

A potential path to finding signatures that may more easily differentiate between different RR and NLCS models is to look at the angular spectra of the scattered photons. Angular spectra have previously been proposed as a way of observing signatures of radiation reaction [30]. This is not something that is typically modelled because PIC codes have generally made the co-linear emission approximation, where photons are emitted directly along the path of particle propagation. PIC codes have an angular spread in emission due the classical dynamics of the electron oscillating in the laser field, but do not resolve the stochastic angle of emission. While this approximation is accurate for high energy photons because the cone of emission goes as $\langle\phi^2\rangle = 5/4\gamma^2$ for $\chi_e \ll 1$ and $\langle\phi^2\rangle = 1.76\gamma^{-2}\chi_e^{2/3}$ for $\chi_e \gg 1$ [31], it is not accurate for the low energy photons. In this manuscript the signatures of the different models of RR that manifest in the photon angular spectrum will be identified and explored under various experimental conditions. This will be done over a large parameter range, taking into account the error associated with real measurement techniques, thereby allowing us to define the minimum laser and electron beam parameters necessary to measure differences in the RR models.

The paper is organized as follows. In section II we discuss the methods employed in this study. The main results are presented in section III. We conclude in section IV.

II. METHODS

Since the main goal of this paper is to study the collision of GeV-class electron beams with high-intensity

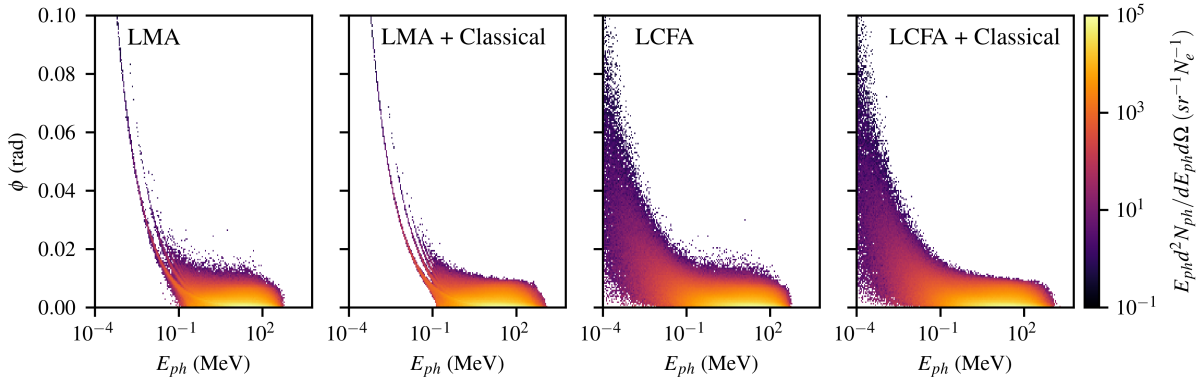

FIG. 1. Characteristic NLCS photon angular spectra generated in Ptarmigan using the LMA, LMA + Classical, LCFA, and LCFA + Classical radiation models. These spectra were generated in the head-on collision of a collimated 1 GeV monoenergetic electron beam with a 27 fs FWHM duration laser with a normalized vector potential $a_0 = 15$. The spectra are normalized to the number of electrons in the colliding beam N_e.

laser pulses in computer simulations, the single-particle Monte Carlo code Ptarmigan was chosen. This code was specifically created for modeling such an interaction and includes multiple models to account for the charged particle and photon interactions with strong electromagnetic fields of laser pulses. The details of the Ptarmigan implementation have been outlined by Blackburn *et al.* [32]. The code can treat the interaction classically, i.e., describe the particle propagation using the Landau-Lifshitz equation of motion. Another possibility is to use the quantum description. In this case the charged particles emit photons and the photons convert into electron positron pairs according to the non-linear Compton and Breit-Wheeler rates that are calculated by the Monte Carlo QED module. The motion of charged particles between emissions is governed by classical equations of motion with only the Lorentz force taken into account. The emission of photons is described in either the LMA or LCFA. The NLCS and NLBW rates include energy and angular dependencies. Since Ptarmigan is a single-particle code and the laser pulse is initialized as a prescribed external field, collective effects and self-consistent field evolution are not taken into account. However, the parameters of laser pulses and electron beams used in this paper allow us to neglect these effects and are therefore comparable to results that would be obtained from QED-PIC codes.

For all the simulations presented here, an electron distribution with a gaussian temporal and spatial profile was populated using 10^5 particles unless specified otherwise. The beam had a variable energy spread defined by the standard deviation σ_E, length $L_e = 2$ μm defining the standard deviation of the longitudinal profile consistent with the short duration of laser wakefield accelerated electron beams [33], a variable mean Lorentz factor $\langle\gamma_e\rangle$, radius $r_e = 0.5$ μm defining the standard deviation of the transverse profile, and variable RMS divergence σ_d. The electron beam was set to propagate head-on into a gaussian laser pulse. This laser pulse had a variable normalized vector potential a_0, wavelength $\lambda = 800$ nm, waist $w_L = 1.7$ μm defining the point where the intensity falls to $1/e^2$ from the peak, full-width half-maximum (FWHM) duration $\tau_{FWHM} = 27$ fs, and was linearly polarized. Note that petawatt laser systems have already been focused to similar spot sizes [10, 34]. The radius of the electron beam was set to be smaller than the laser beam waist such that the electrons would interact with the strongest fields of the pulse. However, laser-wakefield accelerated electron beams can have very small radii [35, 36]. Electrons were individually sent through the fields of the laser pulse. The laser and electrons propagate toward each other and collide at the position where the laser is focused. The motion of particles is calculated by the relativistic Lorentz force equation if the LMA or the LCFA are used and the Landau-Lifshitz equation of motion if the classical solver is used. During the propagation of the particle through the laser fields on each timestep the probability of photons being generated is checked. If a photon is generated, the angle and energy of the photon are calculated pseudo-randomly based on rate tables for LCFA, LMA, or classical versions of these two models. Using classical with LCFA will use the momentum of the electron and the local χ_e of the background field to sample from the classical synchrotron spectrum. Classical combined with LMA takes the normalized vector potential and χ_e to sample the nonlinear Thomson spectrum. If radiation reaction is turned on, the emitting particle will receive a momentum kick due to photon emission. Additionally, the momentum from the absorption of photons from the background is taken into account, however laser depletion is not included. Photons that are generated will propagate through the laser fields and randomly generate electron-positron pairs based on NLBW rates. These generated particles will also propagate through the fields, allowing for the generation of pair-cascades.

III. IDENTIFYING SIGNATURES

Here, we consider the head-on collision of a monoenergetic 1 GeV collimated electron beam with a high intensity ($a_0 = 15$) laser pulse with FWHM duration of 27 fs. The peak value of the parameter χ in such interaction can reach $\chi = 0.18$. Thus, different assumptions can be used to model this interaction. In what follows we employ both the LMA and LCFA, and the classical implementations of these models, i.e. neglecting photon recoil. Previous studies of this interaction typically used angularly integrated spectra, which were able to identify differences in the predictions of these models, but also missed other signatures. It is well known that classical models predict higher emitted photon energies than quantum ones and the LCFA predicts a higher number of low energy photons emitted than the LMA. However, classical models also predict a sharp cut-off in emission angle for a particular energy, whereas quantum ones do not have such a cut-off. The LMA predicts a broader energy distribution of photons at low energies than the LCFA does, although the LMA shows no photons near the axis, in contrast to the LCFA. One of the more interesting distinctions between LCFA and LMA methods is the latter prediction of harmonics in the photon spectra, which appear as multiple curves in the angularly resolved spectrum. Indeed, measuring these harmonics in the QED regime is one of the primary goals of the LUXE experiment [37]. Fig. 1 shows the photon angular spectra for the four different possible radiation models that demonstrate these signatures. In what follows we consider these signatures in detail.

A. Harmonics

1. Structure

The harmonics in LMA come from the scattering of s background photons and can be shown analytically through energy-momentum conservation which is written as follows:

$$q + sk = q' + k'. \tag{1}$$

Here, $q = p + ka_0^2m^2/(2k \cdot p)$ and q' are the quasi-momentum of the electron before and after scattering, with an initial four-momentum p. This electron scatters s background photons with a four-momentum k into a photon with four-momentum k'. By squaring Eqn. 1 and removing q' by plugging Eqn. 1 into the squared equation, we can solve for the angle dependent photon frequency. Specifically for the case of a head-on collision with a highly relativistic beam assuming small angle scattering the solution is:

$$\nu'(\phi) = \frac{8s\nu\gamma^2}{2 + 2\phi^2\gamma^2 - \phi^2 + (4s\nu\gamma + a_0^2)(2 - \frac{\phi^2}{2})}, \tag{2}$$

where $\nu = \hbar\omega/mc^2$ is the normalized frequency. At a particular angle ϕ with respect to the initial electron propagation direction the energy of the scattered photon will increase with the number of background photons scattered. However, the energy change between harmonics decreases with increasing harmonic order.

For the collision of a monoenergetic 1 GeV beam with an $a_0 = 15$ pulse, shown in Fig. 1, clear separations are observed in the 1 – 100 keV range. In this range, photons can be measured directly onto an x-ray camera, or onto a scintillator that is imaged by a camera. If a camera were to image the photons off-axis and resolve the photon spectrum, a multi-peaked spectrum should be measurable. However, this assumes that the peaks in the spectrum can be resolved and that the peaks will not merge together under realistic experimental conditions [38]. Additionally, the signal of each peak will be lower than the previous order, because the scattering probability decreases with increasing harmonic order.

To study the harmonics under realistic experimental conditions we performed several parameter scans of a_0, beam divergence, beam energy, and energy spread using the LMA model. Fig. 2 shows several sample spectra from these scans to demonstrate the trends. As a_0 is increased, the width of the harmonic lines increases and the number of photons scattered to larger angles and into higher harmonics increases. This is expected due to the a_0 dependence in Eq. (2), showing a decrease in scattered photon energy with increasing a_0. The contribution to the width of the harmonic lines due to a_0 can be approximated by taking the difference between Eq. (2) when $a = 0$ and when $a = a_0$. Additionally, the change in energy between two harmonics for a particular ϕ, taking into account a_0 can be estimated by taking the difference between Eq. (2) substituting $s \to s + 1$ and $a = a_0$, and Eq. (2) with $a = 0$. To estimate the lower limit where the harmonics become separate and therefore potentially measurable, we can set this equation equal to 0, to get:

$$\phi_{cross}(s, a_0, \beta) = \cos^{-1}\left(\frac{2 - sa_0^2(1-\beta)}{sa_0^2(1-\beta) + 2\beta}\right). \tag{3}$$

An example of this equation along with the harmonic lines is shown in Fig. 3. If a_0 is small, then the s and $s+1$ harmonic lines will not cross and ϕ_{cross} will be imaginary. This does not account for the complete width of the lines because multiple scattering causes a reduction in γ and therefore an increase in line width. However, using this equation we can estimate the minimum angle that a detector can be placed at to observe separate harmonics.

The scan of γ shows a particularly interesting result. As γ decreases more harmonics appear at larger angles, potentially making the measurement of these harmonics possible. However, reducing γ also reduces the energy at which the harmonic lines are separated. A balance must then be met between having a small enough γ such that the photons are not along the beam propagation axis, but large enough that the harmonics form at energies that are

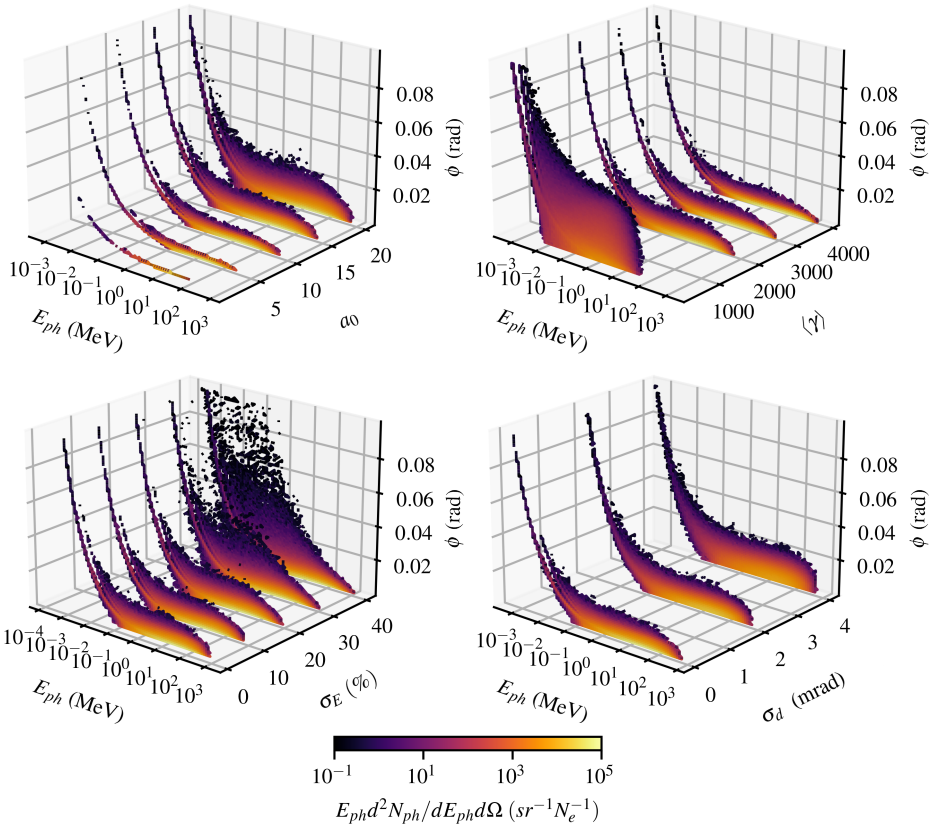

FIG. 2. Scans of a_0, $\langle\gamma\rangle$, divergence angle σ_d, and energy spread σ_E. The base simulation is a monoenergetic 1 GeV beam interacting with a 27 fs, $a_0 = 15$ linear polarized laser using the LMA.

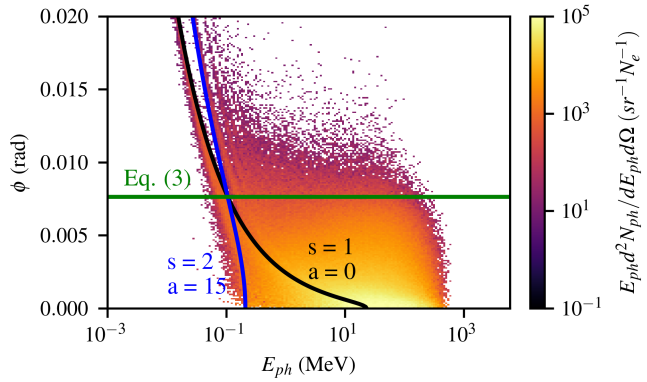

FIG. 3. LMA simulation presented in Fig. 1 ($a_0 = 15$ pulse colliding with 1 GeV beam) plotted with harmonic lines from Eq. (2) and crossing point predicted from Eq. (3).

detectable by a chosen detector. Additionally, a large a_0 is necessary such that there is a significant probability of photons being scattered into the harmonic lines. In plasma physics we generally view a_0 as a measure of how relativistic an interaction is, however a_0 also defines how many photons a single electron will interact with. This point was discussed in the work of Seipt *et al.* [39], where they derived the equation for the average or expectation value of s. This equation is:

$$\langle s\rangle_e = 0.54\frac{a_0^3}{1+1.49\chi_e^{0.59}}, \tag{4}$$

where $\chi_e = 2\gamma_e a_0\hbar\omega/m_e c^2$. From this equation we see that the average s increases with a_0 and decreases with γ consistent with our simulations. The equations defining the probability of emitting into a particular harmonic are not simple [23]. Ptarmigan integrates the partial probabilities of the harmonics to determine whether a photon should be emitted and the energy of the photon [40]. However, for typical parameters of current laser facilities quantum corrections may be small, therefore estimates for the rates may be obtained from the classical equations [41].

For measuring the harmonics we must also consider how energy spread and divergence will affect the harmonic lines. As seen in Fig. 2 both of these properties act to broaden the harmonics, however they appear in different ways. Divergence broadens the lines, causing all the harmonics to merge into a single line for divergences exceeding a few mrad. Energy spread appears to form a background of photons between the lines, however even at largest energy spread in our scan (40%) the lines can still be distinguished. From our scans, divergence angles $\sigma_d \lesssim 2$ mrad and energy spreads less than

20% are necessary to form distinct harmonic lines. Note that σ_E is the standard deviation, for 20% this translates to a $\sim 33\%$ FWHM energy spread. Several experiments have been run demonstrating high quality beams that can meet these requirements [42–44].

Finally note that all simulations were performed in a head-on collision with the electron beam colliding with the laser pulse at focus. Experimental constraints will likely not allow for exact head-on collisions and there will be an angle between the laser pulse and electron beam. This angle will result in a reduction to the χ_e that the electrons experience. Additionally, shot-to-shot variation in the timing and pointing of the beams will result in a reduction of the peak field and therefore χ_e experienced by the electrons. These effects will all result in fewer photons being radiated.

2. *Detection Strategies*

Now that we have established how the harmonics vary with beam and laser properties we can consider how they might be detected. The harmonics form in the 1-100 keV range which is the same range betatron radiation from laser-wakefield acceleration falls into. This complicates the measurement in common laser-driven setups because betatron radiation will form a strong source of noise. If the beam comes from a conventional linear accelerator this will not be a problem. The benefit of betatron existing in this range is that there has already been some effort to develop diagnostics. Albert *et al.* used a stack of image plates to obtain angular spectra of the photons in the keV range [45]. However, the analysis technique requires an assumption on the shape of the spectra and is therefore not applicable to the measurement of harmonics where we are attempting to directly measure the spectral shape. Another method is to diffract the scattered photons from a crystal. This measurement allows for a very narrow range of photon energies to be measured with high resolution. Although this could be quite a good technique for measuring single spectral lines, it is not ideal if we want to fully resolve the harmonics. The best option may be to use single photon counting to construct the spectrum. This method was used by Behm *et al.* to measure differences in betatron spectra transmitted through thin Al foils [46].

For the single photon counting method we consider placing a detector somewhere off the collision axis such that it collects only part of the scattered photons. From the simulations we can create synthetic data to assess the viability of this method. The synthetic detector is created by placing a plane at some position and mapping the position of all photons incident on the plane. A 2D histogram is then created where the size and number of bins is based on a particular x-ray CCD. We have assumed the same CCD as used by Behm *et al.* [46], the Andor iKon-M which which has a 13.3×13.3 mm^2 detector with 1024×1024 pixels. A linear response has been assumed for the detector i.e., the CCD counts of a pixel are linearly proportional to the energy of the incident photon. This is also approximately true for real detectors, however there will also be diffusion of charge from pixels into other pixels and quantum noise that will result in error on the pixel value. The main requirement of this method is to have few photons incident in a single shot such that multiple photons do not hit the same pixel, however enough photons such that the spectrum can be resolved. To reduce the photon density the detector can simply be moved away from the interaction. This will reduce the signal which can be solved by integrating multiple shots. For Fig. 4 the detector has been placed at an angle and at a distance from the interaction where there is a clear separation between the harmonic lines. The part of the spectrum that is captured is enclosed by the blue lines in (a) and (b). Experimentally, the detector should be placed such that the harmonic lines exist in the working range of the detector ($\sim 5 - 15$ keV), far enough away such that fewer than 10% of pixels have non-zero signal, and at a position where the spectral lines are still resolved even with the ~ 0.5 keV spectral resolution of this method. Note that in Fig. 4 the electron beam energy (400 MeV) and $a_0 = 20$ were specifically chosen such that the harmonics would fall within the keV range with clear separation between the lines. To simulate the measurement of the spectra, the 2D synthetic detector histogram was used to generate a 1D histogram with 0.5

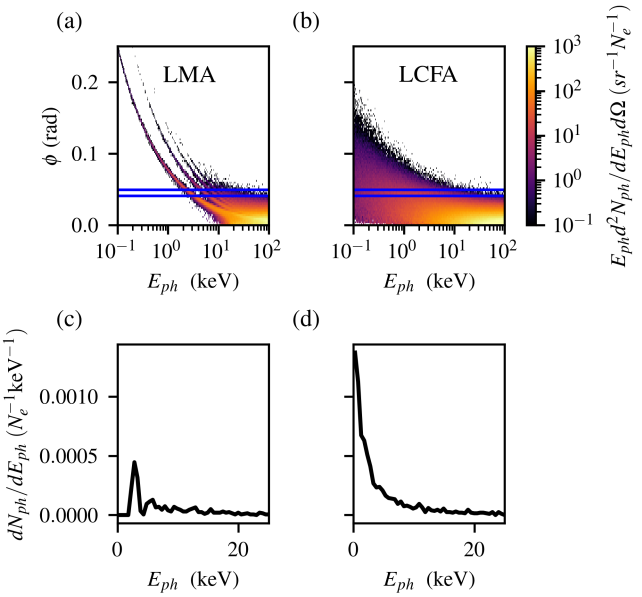

FIG. 4. Synthetic detector measurement of harmonics through single photon counting. The detector is modeled based on the Andor Ikon-M with 1024×1024 pixels placed 1.5 m and 45 mrad from the collision axis. The simulations were run using the LMA model (left column) and LCFA (right column) with $a_0 = 20$ pulse colliding with a 400 MeV monoenergetic electron beam consisting of 4×10^5 particles. The detector captures the angles enclosed by the blue lines.

keV bins. This is shown for the LMA and LCFA spectra in Fig. 4(c) and (d) respectively. From this comparison it is clear that the important measurement is the absence of photons because LCFA predicts a smooth spectrum while LMA has regions between the harmonics with few photons.

An experiment that implements this single photon counting technique to differentiate between the LCFA and the LMA would need to prove with sufficient statistics that the keV part of the scattered spectrum is modulated. Due to shot-to-shot fluctuations, ideally the spectrum would be sufficiently resolved on a single shot. Accumulating over several shots is possible, however it will result in a blurring of the spectral lines as the angle of the beam changes. This can be achieved by placing the detector close enough to the interaction that there is a large flux of photons, but not too close that there are a significant number of multiple hits on the pixels. Additionally, by moving the detector closer, the range of angles captured by the detector increases, and because the harmonic lines are not vertical (Fig. 4) this will increase the linewidth in the angularly integrated spectrum. This set of opposing factors leads to an optimization problem for the detector position. Experimentally, the position of the detector can be scanned to obtain sufficient statistics and separation between harmonics. Note that Fig. 4 effectively shows the result of a single shot with only 4×10^5 electrons. LWFA electron beams are routinely produced with beam charges >pC or $> 6.25 \times 10^6$ electrons. It is therefore likely that sufficient signal can be obtained in a single shot given that a significant fraction of the electrons interact with the laser pulse.

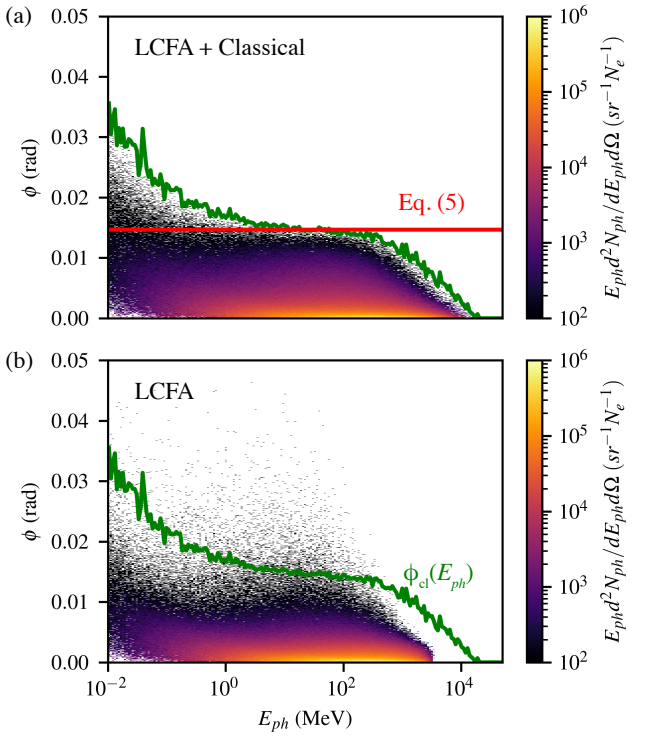

FIG. 5. Classical and quantum photon angular spectra. A line was fit to the classical ϕ_{cl} edge and plotted over the quantum spectrum to demonstrate the existence of photons above this edge. In the MeV range ϕ_{cl} can be approximated by Eq. (5) as shown in (a). The simulations used $\gamma = 7814$ and $a_0 = 26$.

B. Angular Cutoffs

1. *Maximum*

The next signature that we can consider is the hard edge in the radiated photon spectra that forms with CRR, but does not form with QRR. Classically, photon emission is deterministic and neglecting the intrinsic emission cone photons will not be emitted outside an angle $\phi_{edge} = a_0 g(\xi_{max})/\gamma(\xi_{max})$, where ξ_{max} is the phase in the laser field where ϕ_{edge} is maximized, and $g(\xi)$ is the laser envelope. For a laser pulse with a gaussian temporal envelope we can derive the following estimate for the angle of the edge,

$$\phi_{edge} \approx 0.891 \frac{a_0}{\gamma_0}\left(1 + 0.628 \frac{\alpha_f a_0^2 \gamma_0 \hbar\omega}{m_e c^2} N\right). \quad (5)$$

Here, γ_0 is the initial Lorentz factor of the beam, α_f is the fine structure constant, and N is related to the FWHM duration by $N = \omega\tau_{FWHM}/\sqrt{2\ln(2)}$. See Appendix A for the derivation of this equation. This hard edge does not exist in the case of QRR where stochastic effects allow for photons to appear at larger angles. Green and Harvey previously considered the effect of stochastic emission on the transverse momentum of electrons and showed that transverse beam spread may be a measurable signature of QRR [47].

We know that the classical description of photon emission cannot be correct because it allows for the production of photons with energies exceeding the energy of the incoming electron. This can be seen in Fig. 5 where LCFA+Classical over-predicts the maximum photon energy. However, it is not simple to experimentally discriminate between CRR and QRR from the difference in the predicted photon spectra and the resulting difference in the electron spectra. Indeed, this was attempted in the work of Cole *et al.* [24], while the data clearly showed evidence of radiation reaction, it was insufficient to determine the radiation model. Perhaps the photon angular spectra may allow us to discriminate between the models.

To study this we first fit a line to the classical edge to generate the line $\phi_{cl}(E_{ph})$. This is shown in Fig. 5(b) plotted over the quantum spectrum. Note again that classically photons cannot exist at larger angles than this line, however QRR predicts many photons outside of this line, particularly in the 1-100 MeV range. Due to the energy of these photons we cannot use the same single photon counting method that we proposed to measure the

harmonics. Instead, this range requires the use of scintillators, perhaps CsI or LYSO. Arrays of CsI crystals have already been used to measure non-linear Compton spectra [24]. This type of detector was reported by Behm *et al.* as a way to resolve spectra in the MeV range [48]. Measuring spectra with this detector is non-trivial and requires prior knowledge of spectral shape. We can envision placing this detector at a specific scattering angle such that it captures photons only above the classical edge. This angle can be estimated by Eq. (5). As an example, this equation has been used to plot a line in Fig. 5(a) which shows reasonable agreement in the 1 – 100 MeV range. If photons are detected with a spectral shape and number that is consistent with QRR, then this can be used to discriminate between the radiation models. For this measurement to be possible the number of photons above the classical edge must be sufficient to be detectable above the background. The MeV range of photons exist at very small scattering angles, therefore electrons which may scintillate should be deflected away.

To understand what beam and laser parameters are necessary to measure the classical edge we again performed several simulations scanning these properties. The results of these scans are shown in Fig. 6. The important quantity that we focused on in the scans is the number of photons above the classical edge. The number of photons above the line $\phi_{cl}(E_{ph})$ that was fit to the classical simulation for energies $E_{ph} > 0.1$ MeV were integrated and normalized to the total number of photons in the quantum simulation with energies $E_{ph} > 0.1$ MeV. Fig. 6(a) shows this quantity varying with a_0 and $\langle\gamma\rangle$. At low a_0 and $\langle\gamma\rangle$, increasing these parameters results in a larger number of photons above the classical edge. However, the percentage of photons peaks when $\chi_e \approx 0.6$ and falls off for larger χ_e. For small a_0, the classical and quantum spectra appear to be very similar, with the main difference appearing as the shift in the peak energy of the spectrum. Very few photons are observed outside the classical ϕ_{cl} line. Increasing $\langle\gamma\rangle$ decreases the angle of ϕ_{cl} while increasing a_0 increases this angle. Near the peak at $\chi_e = 0.6$, the angle of the classical edge and the angular extent of the quantum spectrum are such that a small fraction of photons in the quantum spectrum have angles that exceed ϕ_{cl}. As $\langle\gamma\rangle$ and a_0 further increase, a very low photon number tail forms. At $\langle\gamma\rangle = 7814$ the maximum scattering angle of MeV photons in the LCFA+Classical simulation increases from ~ 5 mrad at $a_0 = 16$ to $\phi \approx 15$ mrad at $a_0 = 26$. Although QRR predicts an even longer tail in the angular spectra, the photon number in this tail is very small, resulting in the dependence seen in Fig. 6. Fig. 6(a) was generated using a monoenergetic, collimated beam, however a finite energy spread and divergence will affect the measurement. Indeed, in Fig. 6(b) we see that divergence and energy spread result in fewer photons existing above the classical edge. This is because the position of the classical edge is defined by the divergence angle for large divergence angles. For energy spreads $\sigma_E > 20\%$ and divergence angles

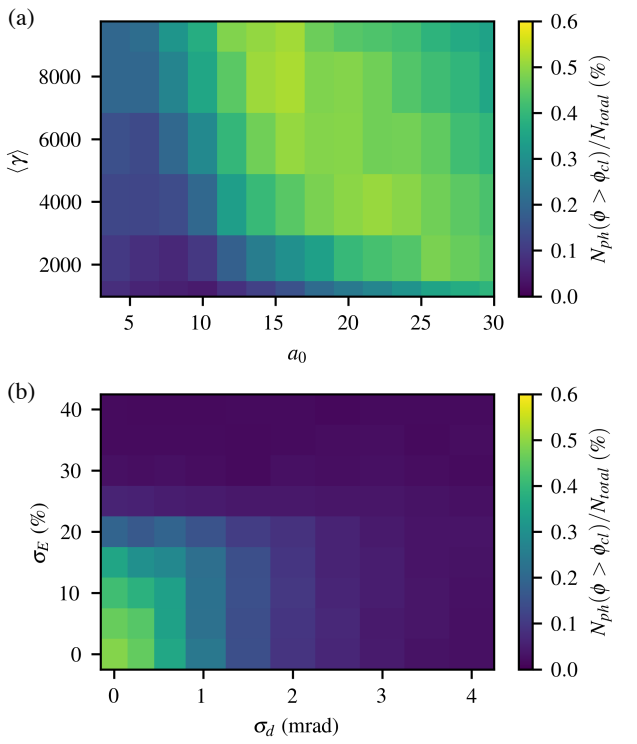

FIG. 6. Percentage of photons above the classical edge ϕ_{cl} for $E_{ph} > 0.1$ MeV using the LMA for $a_0 \leq 10$ and the LCFA for $a_0 > 10$. In (a) a_0 and $\langle\gamma\rangle$ are varied for a collimated monoenergetic beam. In (b) divergence σ_d and energy spread σ_E are scanned for an $a_0 = 18$ laser colliding with a $\langle\gamma\rangle = 5860$ beam.

$\sigma_d > 2$ mrad, almost no photons exist above the edge. Without taking into account how these photons would be detected, this therefore places a limit experimentally on the necessary beam properties. However, it has already been shown that such parameters can be achieved with very high beam energies [44].

2. *Minimum*

The final signature that we will consider is the lower edge of the angular emission for the LMA and the LCFA. In section III A we considered the separation between the harmonics as a signature to differentiate between the LMA and the LCFA, however, the angle of emission that the LCFA predicts also appear over a larger range of scattering angles at a particular energy. In Fig. 1, in the keV range LCFA predicts photons scattered to angles closer to the axis of propagation. If we consider only photons with energies $E_{ph} < 10$ keV being detected on a CCD, the LMA will predict an on-axis hole in the spatial profile of the photons while the LCFA predicts photons covering the detector, however the maximum of the spatial profile does not necessarily occur on-axis. While this signature then seems very promising from a measurement perspec-

tive, it is actually made very difficult by other sources of radiation. If a laser-wakefield accelerated electron beam is used for the collision, betatron radiation will appear on-axis and fill in the x-ray spatial profile. Therefore, experimentally the spatial profile will appear to be similar to that of LCFA regardless of whether it is actually correct. Note however, that a carefully controlled experiment may switch the laser on and off to distinguish the betatron radiation background. Additionally, "beyond LMA" theory predicts the generation of a low energy on-axis population of photons that arises from the temporal envelope of the pulse [49]. The best signature that may allow us to validate the LCFA and the LMA is therefore the harmonics as we previously described. However, in the case of a conventional accelerator betatron x-ray radiation is not generated and this signature may be more easily measurable.

IV. CONCLUSIONS

In this paper, the interaction of a high energy electron beam with a high intensity laser pulse was considered. The head-on collision of these beams is one of the basic configurations to study SFQED effects and has therefore received significant attention recently.

The primary goal of the present study was to identify experimentally measurable signatures that may help to distinguish between different theoretical and simulation models and approximations being used to describe this interaction (see Table I for a summary). Since the parameters of the electron beam and the laser pulse were chosen to be quite moderate, the interaction parameter space was within the applicable range of several models and approximations. The interaction can be described in the framework of classical electrodynamics, using the Landau-Lifshitz equation of motion for electrons, since $\chi_e < 1$. However it can also be described using the methods of SFQED to calculate the rates of photon emission and the modification of the electron four-momenta due to this process. The motion of electrons between the emissions is then governed by the classical equations of motion with only Lorentz force taken into account.

While a few signatures were identified, the measurement of harmonics appears to be the most promising in differentiating between the LCFA and LMA models that have yet to be experimentally validated. By creating a synthetic detector with realistic parameters we showed that single photon counting can resolve the harmonics predicted by the LMA. This measurement will require a small electron beam divergence $\sigma_d \lesssim 2$ mrad and energy spread $\sigma_E \lesssim 20\%$. The laser intensity should be maximized such that there are sufficient photons, while the energy of the electron beam should be optimized such that the harmonics fall within the measurable range of the detector and are well resolved. These parameters are within the capabilities of current multi-petawatt facilities and therefore can be immediately tested at these facilities.

To distinguish between quantum and classical radiation models using the angular spectra, we identified a hard upper limit to the angular emission in the classical spectra that does appear in the quantum spectrum. We also derived an equation to estimate the angular position of this edge. Experimentally, a scintillator could be used to measure photons that appear at angles larger than this estimated angle. However, this measurement will again be affected by the beam and laser parameters. We found that an electron beam divergence $\sigma_d \lesssim 2$ mrad and energy spread $\sigma_E \lesssim 20\%$ are required for this edge to be detectable. The number of photons above this edge is maximized when $\chi_e \approx 0.6$. These parameters are similar to those required to resolve the harmonics except for the beam energy which should be large to resolve the classical edge. However, these parameters are again within the range of what can be achieved at multi-petawatt laser facilities.

ACKNOWLEDGEMENTS

The authors would like to acknowledge useful discussions with Jaroslav Nejdl. This work was supported by the National Science Foundation and Czech Science Foundation under NSF-GACR collaborative grant 2206059 from the NSF and Czech Science Foundation Grant No. 22-42963L. Additionally supported by NSF grant 2108075. SSB was supported by U.S. Department of Energy Office of Science Offices of High Energy Physics and Fusion Energy Sciences (through LaserNetUS), under Contract No. DE-AC02-05CH11231. C.P.R and C.A. supported by UK EPSRC grant EP/V049461/1.

APPENDIX A: CRR MAXIMUM ANGLE DERIVATION

In the angular spectrum with classical radiation reaction we observed a hard cutoff in the maximum angle of emission. To derive the angle of this edge we first start by noting that the angle of emission for an ultrarelativic electron beam propagating through a laser pulse using the small angle approximation is given by,

$$\phi(\xi) = \frac{a_0 \cos(\xi) g(\xi)}{\gamma(\xi)}, \tag{6}$$

where $g(\xi)$ is the longitudinal profile of the pulse and $\xi = 2\omega t$ is the phase for an electron colliding head-on with a laser pulse. Classical radiation reaction will result in the Lorentz factor of the beam decreasing from the original value γ_0 as,

$$\gamma(\xi) = \frac{\gamma_0}{1 + \gamma_0 R I(\xi)}, \tag{7}$$

$$R = \frac{2\alpha_f a_0^2 \hbar\omega}{3mc^2}, \tag{8}$$

Models	Signature	Detection Method	Requirements
LCFA vs. LMA	keV harmonics	X-ray CCD (single photon counting)	Well positioned detector, small divergence and energy spread electron beam
LCFA vs. LMA	keV on-axis hole	X-ray CCD (spatial measurement)	Well characterized background
CRR vs. QRR	MeV edge	CsI scintillator array	Small divergence and energy spread electron beam, high angular resolution detector

TABLE I. Summary of signatures and proposed measurement techniques for differentiating between NLCS and RR models.

$$I(\xi) = \int_{-\infty}^{\xi} g(\xi')^2 d\xi'. \tag{9}$$

Assuming that photons are generated parallel to the instantaneous angle of the electron, the angle of the emitted radiation cannot exceed,

$$\phi_{edge} = \frac{a_0 g(\xi_{max})}{\gamma(\xi_{max})}, \tag{10}$$

where ξ_{max} is the phase that maximizes this equation. This is found by solving,

$$\frac{a_0}{\gamma_0} g'(\xi) + \frac{2\alpha_f a_0^3 \omega}{3mc^2}[g'(\xi) I(\xi) + g(\xi)^3] = 0, \tag{11}$$

where the primes denote differentiation with respect to ξ. To solve this we will use a gaussian pulse where $g(\xi) = \exp(-\xi^2/N^2)$. N can be expressed in terms of the FWHM temporal duration of the pulse τ_{FWHM} as $N = \omega\tau_{FWHM}/\sqrt{2\ln(2)}$. An exact analytical solution cannot be found, however an approximate solution can be found by assuming N is sufficiently large (and radiation reaction sufficiently strong) that expanding in powers of $1/N$ and keeping terms up to $\mathcal{O}(1/N^2)$ is accurate. Providing that $\alpha_f \neq 0$ this results in,

$$\xi_{max} = \frac{\sqrt{2\pi + 80} - \sqrt{2\pi}}{20} N + \cdots \approx 0.339N \tag{12}$$

Substituting this back into Eq. 10 results in the approximate position of the classical edge,

$$\phi_{edge} \approx 0.891 \frac{a_0}{\gamma_0} \left(1 + 0.628 \frac{\alpha_f a_0^2 \gamma_0 \hbar\omega}{m_e c^2} N\right). \tag{13}$$

[1] C. N. Danson, C. Haefner, J. Bromage, T. Butcher, J.-C. F. Chanteloup, E. A. Chowdhury, A. Galvanauskas, L. A. Gizzi, H. J., D. I. Hillier, N. W. Hopps, Y. Kato, E. A. Khazanov, R. Kodama, K. G., R. Li, Y. Li, J. Limpert, J. Ma, C. H. Nam, D. Neely, D. Papadopoulos, R. R. Penman, L. Qian, J. J. Rocca, A. A. Shaykin, C. W. Siders, C. Spindloe, S. Szatmári, R. M. G. M. Trines, J. Zhu, Z. P., and J. D. Zuegel, Petawatt and exawatt lasers worldwide, High Power Laser Science and Engineering **7**, e54 (2019).

[2] A. Di Piazza, C. Muller, K. Z. Hatsagortsyan, and C. H. Keitel, Extremely high-intensity laser interactions with fundamental quantum systems, Reviews of Modern Physics **84**, 1177 (2012).

[3] P. Zhang, S. S. Bulanov, D. Seipt, A. V. Arefiev, and A. G. R. Thomas, Relativistic plasma physics in supercritical fields, Physics of Plasmas **27**, 050601 (2020).

[4] A. Gonoskov, T. G. Blackburn, M. Marklund, and S. S. Bulanov, Charged particle motion and radiation in strong electromagnetic fields, Rev. Mod. Phys. **94**, 045001 (2022).

[5] A. Fedotov, A. Ilderton, F. Karbstein, B. King, D. Seipt, H. Taya, and G. Torgrimsson, Advances in qed with intense background fields, Physics Reports **1010**, 1 (2023), advances in QED with intense background fields.

[6] D. A. Uzdensky, Magnetic reconnection in extreme astrophysical environments, Space Sci. Rev. **160**, 45 (2022).

[7] D. Papadopoulos, J. Zou, C. Le Blanc, G. Chériaux, P. Georges, F. Druon, G. Mennerat, P. Ramirez, L. Martin, A. Fréneaux, and et al., The apollon 10 pw laser: experimental and theoretical investigation of the temporal characteristics, High Power Laser Science and Engineering **4**, e34 (2016).

[8] S. Weber, S. Bechet, S. Borneis, L. Brabec, M. Bučka, E. Chacon-Golcher, M. Ciappina, M. DeMarco, A. Fajstavr, K. Falk, E.-R. Garcia, J. Grosz, Y.-J. Gu, J.-C. Hernandez, M. Holec, P. Janečka, M. Jantač, M. Jirka, H. Kadlecova, D. Khikhlukha, O. Klimo, G. Korn, D. Kramer, D. Kumar, T. Lastovička, P. Lutoslawski, L. Morejon, V. Olšovcová, M. Rajdl, O. Renner, B. Rus, S. Singh, M. Šmid, M. Sokol, R. Versaci, R. Vrána, M. Vranic, J. Vyskočil, A. Wolf, and Q. Yu, P3: An installation for high-energy density plasma physics and ultra-high intensity laser–matter interaction at ELI-Beamlines, Matter and Radiation at Extremes **2**, 149 (2017).

[9] J. Bromage, S.-W. Bahk, I. A. Begishev, C. Dorrer, M. J. Guardalben, B. N. Hoffman, J. Oliver, R. G. Roides, E. M. Schiesser, M. J. Shoup III, and et al., Technology development for ultraintense all-opcpa systems, High Power Laser Science and Engineering **7**, e4 (2019).

[10] J. W. Yoon, Y. G. Kim, I. W. Choi, J. H. Sung, H. W. Lee, S. K. Lee, and C. H. Nam, Realization of laser intensity over 10^{23}w/cm^2, Optica **8**, 630 (2021).

[11] J. Nees, A. Maksimchuk, G. Kalinchenko, B. Hou, Y. Ma, P. Campbell, A. McKelvey, L. Willingale, I. Jovanovic, C. Kuranz, A. Thomas, and K. Krushelnick, Zeus: A national science foundation mid-scale facility for laser-driven science in the qed regime, in *2020 Conference on Lasers and Electro-Optics (CLEO)* (2020) pp. 1–2.

[12] K. M. Schoeffler, T. Grismayer, D. Uzdensky, R. A. Fonseca, and L. O. Silva, Bright gamma-ray flares powered by magnetic reconnection in qed-strength magnetic fields, The Astrophysical Journal **870**, 49 (2019).

[13] F. Cruz, T. Grismayer, A. Y. Chen, A. Spitkovsky, and L. O. Silva, Coherent emission from qed cascades in pulsar polar caps, The Astrophysical Journal Letters **919**, L4 (2021).

[14] C. P. Ridgers, R. D. J. G. Kirk, T. G. Blackburn, C. S. Brady, K. Bennett, T. D. Arber, and A. R. Bell, J. Comput. Phys. **260**, 273 (2014).

[15] M. Tanabashi *et al.*, Particle data group, Phys. Rev. D **98**, 030001 (2018).

[16] D. M. Wolkow, Über eine klasse von lösungen der diracschen gleichung, Zeitschrift für Physik **94**, 250 (1935).

[17] L. S. Brown and T. W. B. Kibble, Interaction of intense laser beams with electrons, Phys. Rev. **133**, A705 (1964).

[18] E. S. Sarachik and G. T. Schappert, Classical theory of the scattering of intense laser radiation by free electrons, Phys. Rev. D **1**, 2738 (1970).

[19] V. I. Ritus, Quantum effects of the interaction of elementary particles with an intense electromagnetic field, J. Sov. Laser Res. **6**, 497 (1985).

[20] See the discussion on the definition of a_0 in Refs. [4, 50].

[21] C. Bula, K. T. McDonald, E. J. Prebys, C. Bamber, S. Boege, T. Kotseroglou, A. C. Melissinos, D. D. Meyerhofer, W. Ragg, D. L. Burke, R. C. Field, G. Horton-Smith, A. C. Odian, J. E. Spencer, D. Walz, S. C. Berridge, W. M. Bugg, K. Shmakov, and A. W. Weidemann, Observation of nonlinear effects in compton scattering, Phys. Rev. Lett. **76**, 3116 (1996).

[22] D. L. Burke, R. C. Field, G. Horton-Smith, J. E. Spencer, D. Walz, S. C. Berridge, W. M. Bugg, K. Shmakov, A. W. Weidemann, C. Bula, K. T. McDonald, E. J. Prebys, C. Bamber, S. J. Boege, T. Koffas, T. Kotseroglou, A. C. Melissinos, D. D. Meyerhofer, D. A. Reis, and W. Ragg, Positron production in multiphoton light-by-light scattering, Phys. Rev. Lett. **79**, 1626 (1997).

[23] T. Heinzl, B. King, and A. J. MacLeod, Locally monochromatic approximation to qed in intense laser fields, Phys. Rev. A **102**, 063110 (2020).

[24] J. M. Cole, K. T. Behm, E. Gerstmayr, T. G. Blackburn, J. C. Wood, C. D. Baird, M. J. Duff, C. Harvey, A. Ilderton, A. S. Joglekar, K. Krushelnick, S. Kuschel, M. Marklund, P. McKenna, C. D. Murphy, K. Poder, C. P. Ridgers, G. M. Samarin, G. Sarri, D. R. Symes, A. G. R. Thomas, J. Warwick, M. Zepf, Z. Najmudin, and S. P. D. Mangles, Experimental evidence of radiation reaction in the collision of a high-intensity laser pulse with a laser-wakefield accelerated electron beam, Phys. Rev. X **8**, 011020 (2018).

[25] K. Poder, M. Tamburini, G. Sarri, A. Di Piazza, S. Kuschel, C. D. Baird, K. Behm, S. Bohlen, J. M. Cole, D. J. Corvan, M. Duff, E. Gerstmayr, C. H. Keitel, K. Krushelnick, S. P. D. Mangles, P. McKenna, C. D. Murphy, Z. Najmudin, C. P. Ridgers, G. M. Samarin, D. R. Symes, A. G. R. Thomas, J. Warwick, and M. Zepf, Experimental signatures of the quantum nature of radiation reaction in the field of an ultraintense laser, Phys. Rev. X **8**, 031004 (2018).

[26] J. A. Gaunt and R. H. Fowler, Continuous absorption, Philosophical Transactions of the Royal Society of London. Series A, Containing Papers of a Mathematical or Physical Character **229**, 163 (1930).

[27] V. N. Baier, V. M. Katkov, and V. M. Strakhovenko, *Electromagnetic Processes at High Energies in Oriented Single Crystals* (WORLD SCIENTIFIC, 1998) https://www.worldscientific.com/doi/pdf/10.1142/2216.

[28] C. N. Harvey, A. Ilderton, and B. King, Testing numerical implementations of strong-field electrodynamics, Phys. Rev. A **91**, 013822 (2015).

[29] A. Di Piazza, M. Tamburini, S. Meuren, and C. H. Keitel, Implementing nonlinear compton scattering beyond the local-constant-field approximation, Phys. Rev. A **98**, 012134 (2018).

[30] A. Di Piazza, K. Z. Hatsagortsyan, and C. H. Keitel, Strong signatures of radiation reaction below the radiation-dominated regime, Phys. Rev. Lett. **102**, 254802 (2009).

[31] T. G. Blackburn, D. Seipt, S. S. Bulanov, and M. Marklund, Radiation beaming in the quantum regime, Phys. Rev. A **101**, 012505 (2020).

[32] T. G. Blackburn, B. King, and S. Tang, Simulations of laser-driven strong-field qed with ptarmigan: Resolving wavelength-scale interference and γ-ray polarization (2023), arXiv:2305.13061 [hep-ph].

[33] O. Lundh, J. Lim, C. Rechatin, L. Ammoura, A. Ben-Ismaïl, X. Davoine, G. Gallot, J.-P. Goddet, E. Lefebvre, V. Malka, and J. Faure, Few femtosecond, few kiloampere electron bunch produced by a laser–plasma accelerator, Nature Physics **7**, 219 (2011).

[34] A. S. Pirozhkov, Y. Fukuda, M. Nishiuchi, H. Kiriyama, A. Sagisaka, K. Ogura, M. Mori, M. Kishimoto, H. Sakaki, N. P. Dover, K. Kondo, N. Nakanii, K. Huang, M. Kanasaki, K. Kondo, and M. Kando, Approaching the diffraction-limited, bandwidth-limited petawatt, Opt. Express **25**, 20486 (2017).

[35] R. Weingartner, S. Raith, A. Popp, S. Chou, J. Wenz, K. Khrennikov, M. Heigoldt, A. R. Maier, N. Kajumba, M. Fuchs, B. Zeitler, F. Krausz, S. Karsch, and F. Grüner, Ultralow emittance electron beams from a laser-wakefield accelerator, Phys. Rev. ST Accel. Beams **15**, 111302 (2012).

[36] S. K. Barber, J. van Tilborg, C. B. Schroeder, R. Lehe, H.-E. Tsai, K. K. Swanson, S. Steinke, K. Nakamura, C. G. R. Geddes, C. Benedetti, E. Esarey, and W. P. Leemans, Measured emittance dependence on the injection method in laser plasma accelerators, Phys. Rev. Lett. **119**, 104801 (2017).

[37] H. Abramowicz, U. Acosta, M. Altarelli, R. Aßmann, Z. Bai, T. Behnke, Y. Benhammou, T. Blackburn, S. Boogert, O. Borysov, M. Borysova, R. Brinkmann, M. Bruschi, F. Burkart, K. Büßer, N. Cavanagh, O. Davidi, W. Decking, U. Dosselli, N. Elkina, A. Fedotov, M. Firlej, T. Fiutowski, K. Fleck, M. Gostkin, C. Grojean, J. Hallford, H. Harsh, A. Hartin, B. Heinemann, T. Heinzl, L. Helary, M. Hoffmann, S. Huang, X. Huang, M. Idzik, A. Ilderton, R. Jacobs, B. Kämpfer, B. King, H. Lahno, A. Levanon, A. Levy, I. Levy, J. List, W. Lohmann, T. Ma, A. J. Macleod, V. Malka, F. Meloni, A. Mironov, M. Morandin, J. Moron, E. Negodin,

G. Perez, I. Pomerantz, R. Pöschl, R. Prasad, F. Quéré, A. Ringwald, C. Rödel, S. Rykovanov, F. Salgado, A. Santra, G. Sarri, A. Sävert, A. Sbrizzi, S. Schmitt, U. Schramm, S. Schuwalow, D. Seipt, L. Shaimerdenova, M. Shchedrolosiev, M. Skakunov, Y. Soreq, M. Streeter, K. Swientek, N. T. Hod, S. Tang, T. Teter, D. Thoden, A. I. Titov, O. Tolbanov, G. Torgrimsson, A. Tyazhev, M. Wing, M. Zanetti, A. Zarubin, K. Zeil, M. Zepf, and A. Zhemchukov, Conceptual design report for the luxe experiment, The European Physical Journal Special Topics **230**, 2445 (2021).

[38] A. G. R. Thomas, C. P. Ridgers, S. S. Bulanov, B. J. Griffin, and S. P. D. Mangles, Strong radiation-damping effects in a gamma-ray source generated by the interaction of a high-intensity laser with a wakefield-accelerated electron beam, Phys. Rev. X **2**, 041004 (2012).

[39] D. Seipt, T. Heinzl, M. Marklund, and S. S. Bulanov, Depletion of intense fields, Phys. Rev. Lett. **118**, 154803 (2017).

[40] T. G. Blackburn, A. J. MacLeod, and B. King, From local to nonlocal: higher fidelity simulations of photon emission in intense laser pulses, New Journal of Physics **23**, 085008 (2021).

[41] E. Esarey, S. K. Ride, and P. Sprangle, Nonlinear thomson scattering of intense laser pulses from beams and plasmas, Phys. Rev. E **48**, 3003 (1993).

[42] W. T. Wang, W. T. Li, J. S. Liu, Z. J. Zhang, R. Qi, C. H. Yu, J. Q. Liu, M. Fang, Z. Y. Qin, C. Wang, Y. Xu, F. X. Wu, Y. X. Leng, R. X. Li, and Z. Z. Xu, High-brightness high-energy electron beams from a laser wakefield accelerator via energy chirp control, Phys. Rev. Lett. **117**, 124801 (2016).

[43] A. R. Maier, N. M. Delbos, T. Eichner, L. Hübner, S. Jalas, L. Jeppe, S. W. Jolly, M. Kirchen, V. Leroux, P. Messner, M. Schnepp, M. Trunk, P. A. Walker, C. Werle, and P. Winkler, Decoding sources of energy variability in a laser-plasma accelerator, Phys. Rev. X **10**, 031039 (2020).

[44] B. Miao, J. E. Shrock, L. Feder, R. C. Hollinger, J. Morrison, R. Nedbailo, A. Picksley, H. Song, S. Wang, J. J. Rocca, and H. M. Milchberg, Multi-gev electron bunches from an all-optical laser wakefield accelerator, Phys. Rev. X **12**, 031038 (2022).

[45] F. Albert, B. B. Pollock, J. L. Shaw, K. A. Marsh, J. E. Ralph, Y.-H. Chen, D. Alessi, A. Pak, C. E. Clayton, S. H. Glenzer, and C. Joshi, Angular dependence of betatron x-ray spectra from a laser-wakefield accelerator, Phys. Rev. Lett. **111**, 235004 (2013).

[46] K. Behm, A. Hussein, T. Zhao, R. Baggott, J. Cole, E. Hill, K. Krushelnick, A. Maksimchuk, J. Nees, S. Rose, A. Thomas, R. Watt, J. Wood, V. Yanovsky, and S. Mangles, Demonstration of femtosecond broadband x-rays from laser wakefield acceleration as a source for pump-probe x-ray absorption studies, High Energy Density Physics **35**, 100729 (2020).

[47] D. G. Green and C. N. Harvey, Transverse spreading of electrons in high-intensity laser fields, Phys. Rev. Lett. **112**, 164801 (2014).

[48] K. T. Behm, J. M. Cole, A. S. Joglekar, E. Gerstmayr, J. C. Wood, C. D. Baird, T. G. Blackburn, M. Duff, C. Harvey, A. Ilderton, S. Kuschel, S. P. D. Mangles, M. Marklund, P. McKenna, C. D. Murphy, Z. Najmudin, K. Poder, C. P. Ridgers, G. Sarri, G. M. Samarin, D. Symes, J. Warwick, M. Zepf, K. Krushelnick, and A. G. R. Thomas, A spectrometer for ultrashort gamma-ray pulses with photon energies greater than 10 MeV, Review of Scientific Instruments **89**, 113303 (2018).

[49] B. King, Interference effects in nonlinear compton scattering due to pulse envelope, Phys. Rev. D **103**, 036018 (2021).

[50] T. Heinzl and A. Ilderton, A lorentz and gauge invariant measure of laser intensity, Optics Communications **282**, 1879 (2009).